# Ultrathin layer sensing based on hybrid coupler with short-range surface plasmon polariton and dielectric waveguide

Ruiyuan Wan,[1] Fang Liu,[1,2] and Yidong Huang[1,3]

[1]*Department of Electronic Engineering, State Key Lab of Integrated Optoelectronics, Tsinghua University, Beijing 100084, China*

[2] *liu_fang@tsinghua.edu.cn*

[3] *yidonghuang@tsinghua.edu.cn*

Received August 28, 2009; revised November 16, 2009; accepted November 23, 2009; posted December 18, 2009 (Doc. ID 116389); published January 15, 2010

A highly integrated sensor that is based on a hybrid coupler composed of short-range surface plasmon polariton (SRSPP) and dielectric waveguides was proposed for refractive index detecting of an ultrathin layer. The dependence of the coupling between the SRSPP and dielectric waveguide mode on the refractive index of the detecting layer was analyzed theoretically. For a detecting layer as thin as 1/15 wavelength, the resolution can be as high as $3.3\times10^{-6}$ refractive index units with a sensing length of only tens of micrometers.

*OCIS codes:* 240.6680, 280.4788.

A surface plasmon polariton (SPP) is a transverse magnetic surface electromagnetic excitation that propagates along the interface between a metal and a dielectric medium [1]. Resulting from the mode field concentrated on the metal surface, the SPP is sensitive to the dielectric refractive index change on the metal surface [2]. During the past two decades, its application in chemical and biological sensing has received continuous and extensive attention [2–4]. However, when the molecular interaction occurs within a rather thin layer [3], the actual detecting layer is only about tens or several hundreds of nanometers, in which case the sensitivity of a conventional SPP sensor degrades dramatically. This is because such a thin detecting thickness is much less than the field penetration depth of the general SPP mode.

For a thin metal film embedded in dielectrics, the SPPs on the upper and the lower metal–dielectric interfaces couple and form two modes: long-range SPP (LRSPP) and short-range SPP (SRSPP) modes [1]. The LRSPP, with its mode field extending to surrounding dielectrics, is promising for highly sensitive detection of bulk refractive index change [5]. The SRSPP mode, with its mode field tightly bound to the metal surface, is promising for ultrathin layer detection, which has been illustrated by prism-based [6] and grating-based sensors [7]. Recently, we demonstrated theoretically the highly efficient vertical coupling between the SRSPP and dielectric waveguide (DW) mode [8]. In this Letter, based on this vertical hybrid coupler, a highly integrated sensor is proposed for detecting the refractive index change of an ultrathin layer. The surface refractive index dependence of the coupling between SRSPP and DW modes is analyzed theoretically. It is demonstrated that even for a detecting layer as thin as 1/15 wavelength, the high resolution, up to $3.3\times10^{-6}$ RIU (refractive index units) within the large refractive index range of $3\times10^{-2}$ RIU can be obtained with a sensing length only about tens of micrometers.

The proposed highly integrated sensor based on the SRSPP-dielectric hybrid coupler is shown in Fig. 1. The operating wavelength $\lambda$ is fixed at 1.55 $\mu$m. As shown in the figure, the sensor is composed of the $SiO_2$ substrate (refractive index $n_s=1.444$), $SiN_x$ waveguide layer ($n_d=2$ and thickness $h_d=146$ nm), $SiO_2$ buffer layer ($h_b=2$ $\mu$m), and Au film (dielectric constant $\varepsilon_m=-132+i\times12.65$ [9] and $h_m=22$ nm). Above the Au film is the detecting layer with varied refractive index $n_{det}$ (1.3–1.6) and thickness $h_{det}$ (100–500 nm) in the water environment. The effective sensing length along the $z$ direction is determined by the length of the Au film $L$ [10].

For the SRSPP supported by 22 nm thick Au film embedded in $SiO_2$ when $\lambda=1.55$ $\mu$m, the $1/e$ penetration depth in the dielectric is only about 600 nm, which is much thinner than that of general SPP modes. Therefore, the refractive index change within a rather thin layer would notably influence the coupling efficiency between the SRSPP and DW modes.

The device shown in Fig. 1 can be divided into three regions along the $z$ direction: input region I ($z<0$), sensing region II ($0<z<L$), and output region III ($z>L$). In the sensing region II, there exist two dominant bounded eigenmodes, mode A and B, resulting from the in-phase and opposite-phase coupling between the SRSPP and DW modes. Figures 2(a)–2(d) show the real and nonnegligible imaginary

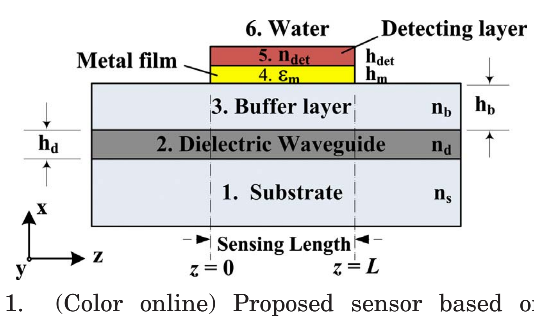


Fig. 1. (Color online) Proposed sensor based on the SRSPP–dielectric hybrid coupling structure.

0146-9592/10/020244-3/$15.00 

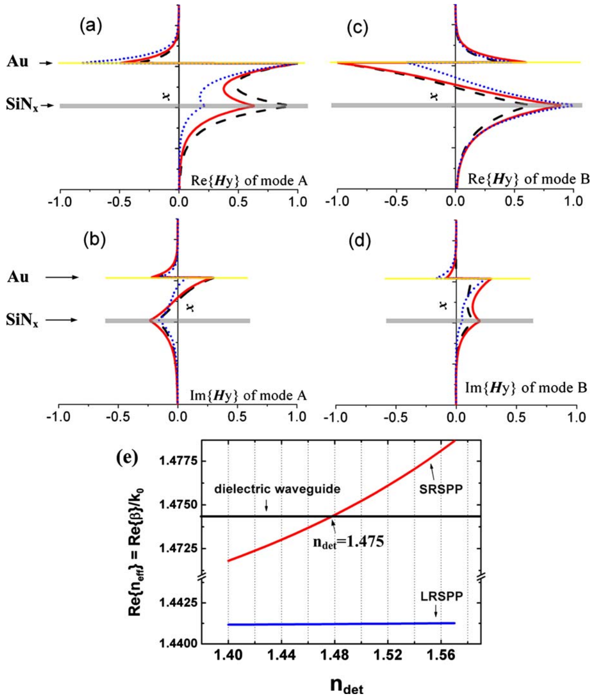


Fig. 2. (Color online) (a)–(d) Complex magnetic field profile of two eigenmodes when $h_{\mathrm{det}}=150$ nm with $n_{\mathrm{det}}=1.4$ (black dashed), $n_{\mathrm{det}}=1.475$ (red solid), and $n_{\mathrm{det}}=1.57$ (blue dotted). (a) and (b) show the real and imaginary part of mode A, respectively; (c) and (d) show the real and imaginary part of mode B, respectively. (e) Effective refractive index (Re$\{n_{\mathrm{eff}}\}$) of SRSPP (red) and LRSPP (blue) mode of individual Au waveguide part (layers 3–6 in Fig. 1) as a function of $n_{\mathrm{det}}$. The black line corresponds to Re$\{n_{\mathrm{eff}}\}$ of the dielectric waveguide mode supported by individual $\mathrm{SiN}_x$ waveguide parts (layers 1–3 in Fig. 1).

part of the main magnetic field component $H_y$ of these two bounded eigenmodes with different $n_{\mathrm{det}}$ when the detecting layer is only 150 nm thick. The red solid profile illustrates that the concentrations of the mode fields surrounding the Au film and DW are almost equal when $n_{\mathrm{det}}=1.475$. In this case, the effective refractive indices (Re$\{n_{\mathrm{eff}}\}$) of individual SRSPP and DW modes match each other well, which corresponds to the crossing point of the black and red curves shown in Fig. 2(e). Reducing $n_{\mathrm{det}}$ to 1.4 or increasing $n_{\mathrm{det}}$ to 1.57 will cause the Re$\{n_{\mathrm{eff}}\}$ of the individual SRSPP mode to deviate from the crossing point, which results in unbalanced field concentrations surrounding the Au and $\mathrm{SiN}_x$ waveguide, as illustrated by the black dashed and blue dotted profiles in Figs. 2(a)–2(d).

As the input, the DW mode $\mathbf{H}_{\mathrm{d}}(x)$ of region I can be expressed in terms of the superposition of the above two eigenmodes $\mathbf{H}_{\mathrm{A}}(x)$ and $\mathbf{H}_{\mathrm{B}}(x)$ of region II at $z=0$,

$$\mathbf{H}(x,z) = \sum_{m=A,B} a_{\mathrm{m}} e^{-\beta_{\mathrm{mi}} z} \mathbf{H}_{\mathrm{m}}(x) e^{-i\beta_{\mathrm{mr}} z}, \tag{1}$$

where $a_{\mathrm{m}}=\frac{1}{2}\int(\mathrm{E_d}\times\mathrm{H_m})\cdot\hat{z}\mathrm{d}x$ and $\beta_{\mathrm{m}}=\beta_{\mathrm{mr}}-i\times\beta_{\mathrm{mi}}$ ($m=\mathrm{A,B}$) are the complex propagation constants of the eigenmodes in region II. Here all the modes are normalized according to the unconjugated versions of Eqs. (11–16) in [11], and $a_{\mathrm{A}}{}^2+a_{\mathrm{B}}{}^2\approx 1$ to ensure the completeness of expanding the input with the two eigenmodes at $z=0$.

After the propagation length $L$, the coefficient of the DW TM mode field $\mathbf{H}_{\mathrm{d}}$ ($\mathbf{E}_{\mathrm{d}}$) in region III at $z=L$ can be expressed as

$$a_L = \frac{1}{2}\int(\mathbf{E}_{\mathrm{d}}\times\mathbf{H}(x,z=L))\cdot\hat{z}\mathrm{d}A = \sum_{m=\mathrm{A,B}} a_{\mathrm{m}}{}^2 e^{-\beta_{\mathrm{mi}}L} e^{-i\beta_{\mathrm{mr}}L}. \tag{2}$$

When the input power of region I is set as 0 dBm, the output power from the DW of region III is $P_{\mathrm{out}}=20\times\log|a_{\mathrm{L}}|$ dBm. According to Eqs. (1) and (2), the $n_{\mathrm{det}}$ dependence of coupling efficiency between the SRSPP and the DW modes can be examined by studying the field intensity transmitting along the $z$ direction and how $P_{\mathrm{out}}$ changes as a function of $L$.

Figure 3(a) shows the output power $P_{\mathrm{out}}$ as a function of $L$ with different $n_{\mathrm{det}}$. It can be seen that, when $n_{\mathrm{det}}=1.475$, the output power declines rapidly along $L$ with strong ripple, and the period of the beat is in close agreement with $2L_{\mathrm{c}}$ (coupling length $L_{\mathrm{c}}=\pi/(\beta_{\mathrm{Ar}}-\beta_{\mathrm{Br}})$). The large decline slope and strong ripple result from the complete energy exchange between the DW mode and high-loss SRSPP mode. This can be understood easily by observing the energy transmission process in the $x$–$z$ plane; it is shown in Fig. 3(c) that the energy of the DW mode transfers completely to the SRSPP mode and then couples back. Compared with Fig. 3(c), Fig. 3(b) illustrates that when $n_{\mathrm{det}}=1.4$, there is always some residual energy remaining in the DW, and total energy decreases slower along $z$. In this case, less energy is coupled to the high-loss SRSPP mode, and the shorter coupling length results in a smaller loss

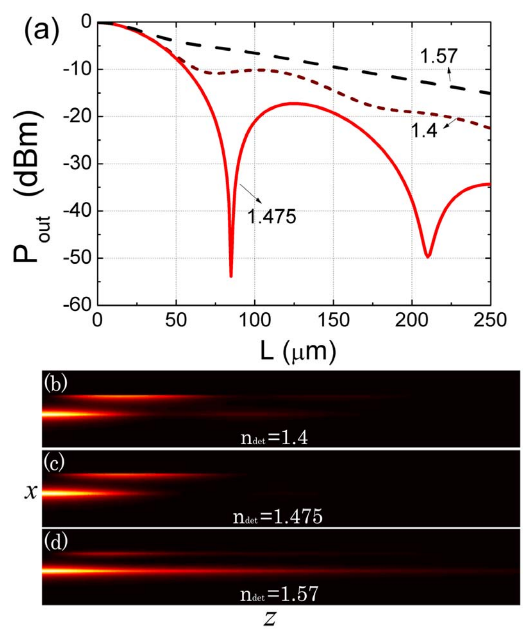


Fig. 3. (Color online) (a) Output power $P_{\mathrm{out}}$ versus sensing length $L$ labeled with different $n_{\mathrm{det}}$. Simulated field intensity transmission process when (b) $n_{\mathrm{det}}=1.4$, (c) $n_{\mathrm{det}}=1.475$, and (d) $n_{\mathrm{det}}=1.57$.

when the energy couples back to the DW. That is the reason why the short-dashed curve shown in Fig. 3(a) has much weaker ripple and smaller slope compared with the solid curve. Similarly, when $n_{\mathrm{det}}$ is increased to 1.57, the coupling is even weaker, with most of the energy propagating through the DW, and the corresponding $P_{\mathrm{out}}$ shown as long-dashed curve in Fig. 3(a) has little ripple and much smaller slope.

Therefore, it can be concluded that the better the mode field concentration around two arms matches, the higher the coupling efficiency is, and the stronger the ripple will appear in the $P_{\mathrm{out}}-L$ curve with a larger decline slope. Here, the extremely weak coupling between LRSPP and DW modes is ignored because of their significant $\mathrm{Re}\{n_{\mathrm{eff}}\}$ difference, shown in Fig. 2(e).

As a result, based on the highly sensitive SRSPP–dielectric coupling characteristics to the refractive index of the thin detecting film, a highly integrated sensor can be realized. Figure 4 shows that the $P_{\mathrm{out}}$ varies dramatically with $n_{\mathrm{det}}$ for different detecting thickness by setting $L=85$ $\mu$m, which corresponds to the leftmost dip in the red solid curve shown in Fig. 3(a). The dips of the curves in Fig. 4 and the variation of the output power over the corresponding change of $n_{\mathrm{det}}$ were defined as the sensing center and sensitivity [2], respectively. The sensitivity for the 100-nm-thick (thinner than 1/15 wavelength) detecting layer was estimated. According to the dotted–dashed curve in Fig. 4, the average sensitivity in the range of $n_{\mathrm{det}}=1.52$ to $n_{\mathrm{det}}=1.55$ can be as high as 2983 dB/RIU. If the resolution of the powermeter is 0.01 dB [2], the minimum detectable refractive index change can be as small as $3.3\times10^{-6}$ RIU. The high resolution for such a thin detecting layer can be attributed to the extremely bound field of the SRSPP mode of the metal film. It should be also noted that such high resolution can be obtained in a large refractive index range of about $3\times10^{-2}$ RIU. This is because the SRSPP can still be supported under the comparatively large refractive index difference below and above the metal film. In addition, according to the results of Figs. 3 and 4, the sensing length can be shorter than 100 $\mu$m owing to the strong coupling between SRSPP and DW modes.

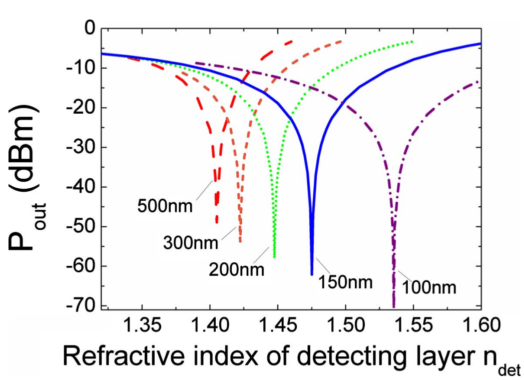


Fig. 4. (Color online) Output power $P_{\mathrm{out}}$ as a function of $n_{\mathrm{det}}$ labeled with different detecting thickness $h_{\mathrm{det}}$.

Therefore, compared with traditional SPP sensors [2–4,6,7,12], the proposed SRSPP–dielectric coupling sensor can have better performance, such as a much more compact size, larger sensing range, and higher sensitivity for detecting films thinner than 1/10 of a wavelength.

It can be also seen in Fig. 4 that, when the thickness of the detecting layer $h_{\mathrm{det}}$ is decreased from 500 to 100 nm, the sensing center shifts from $n_{\mathrm{det}}=1.405$ to the higher value $n_{\mathrm{det}}=1.535$. The shift of the sensing center can be interpreted that the total dielectric refractive index above the metal film decreases with thinner $h_{\mathrm{det}}$. As a result, to get a high coupling efficiency between SRSPP and DW modes, a larger $n_{\mathrm{det}}$ is required for a thinner detecting layer.

In conclusion, a highly integrated sensor based on the coupling between SRSPP and DW modes was proposed for detecting the refractive index change of an ultrathin layer. The dependence of the coupling efficiency between SRSPP and DW modes on the surface refractive index change was analyzed theoretically. It was demonstrated that even for a detecting layer thinner than 1/15 wavelength, a resolution as high as $3.3\times10^{-6}$ RIU within a large refractive index range of $3\times10^{-2}$ RIU can be obtained with a sensing length as short as tens of micrometers. All these advantages meet the requirements for a SPP sensor of the next generation.

This work is supported by the 973 Program of China under contract 2007CB307004 and the National Natural Science Foundation of China (NSFC-60877023). The authors thank Prof. Jiangde Peng, Prof. Wei Zhang, and Dr. Xue Feng for their helpful comments.

## References

1. J. J. Bruke and G. I. Stegeman, Phys. Rev. B **33**, 5186 (1986).
2. J. Homola, S. S. Yee, and G. Gauglitz, Sens. Actuators B **54**, 3 (1999).
3. J. Homola, Anal. Bioanal. Chem. **377**, 528 (2003).
4. X. D. Hoa, A. G. Kirk, and M. Tabrizian, Biosens. Bioelectron. **23**, 151 (2007).
5. F. Liu, R. Wan, Y. Huang, and J. Peng, Opt. Lett. **34**, 2697 (2009).
6. J. Guo, P. D. Keathley, and J. T. Hastings, Opt. Lett. **33**, 512 (2008).
7. M. Vala, J. Dostálek, and J. Homola, Proc. SPIE **6585**, 658522 (2007).
8. R. Wan, F. Liu, X. Tang, Y. Huang, and J. Peng, Appl. Phys. Lett. **94**, 141104 (2009).
9. E. D. Palik, *Handbook of Optical Constants of Solids* (Academic, 1985).
10. J. Dostalek, J. Ctyrok, J. Homola, E. Brynda, M. Skalsky, P. Nekvindova, J. Spikova, J. Skvor, and J. Schrofel, Sens. Actuators B **76**, 8 (2001).
11. A. W. Snyder and J. D. Love, *Optical Waveguide Theory* (Kluwer Academic, 1983), pp. 212–214.
12. M. N. Weiss, R. Srivastava, H. Groger, P. Lo, and S. F. Luo, Sens. Actuators A **51**, 211 (1996).